Catal Lett (2009) 128:164–170
DOI 10.1007/s10562-008-9720-1

Selective Hydrogenation of Nitrobenzene to Aniline over Ru/SBA-15 Catalysts

Komandur V. R. Chary · Chakravartula S. Srikanth

Received: 12 August 2008 / Accepted: 27 September 2008 / Published online: 7 November 2008

Abstract A series of Ru/SBA-15 catalysts (0.5–6.0 wt%) are prepared by impregnation method. The catalysts were characterized by X-ray diffraction (XRD), transmission electron microscopy (TEM), temperature programmed reduction (TPR), X-ray photoelectron spectroscopy (XPS), CO-chemisorption, surface area and pore-size distribution measurements. The catalytic activities were evaluated for the vapor phase hydrogenation of nitrobenzene. The dispersion measured by CO-uptake values suggests decrease in dispersion with increasing Ru loading on SBA-15. These findings are well supported by the crystallite size measured from XRD and TEM measurements. XPS study reveals the formation of Ru0 after reduction at 573 K for 3 h. The catalysts exhibit high conversion/selectivity at 4.5 wt% Ru loading during hydrogenation reaction. The particle size measured from CO-chemisorption and TEM analysis related to the TOF during the hydrogenation reaction. Ru/SBA-15 catalysts are found to show higher conversion/selectivities during hydrogenation of nitrobenzene than Ru/SiO_2 and Ru/Al_2O_3 catalysts.

Keywords SBA-15 · Ruthenium catalyst · Hydrogenation · Nitrobenzene and active sites

1 Introduction

Aniline is a valuable chemical for the plastics, rubber processing, herbicides, dyes and pigments industries. About 85% of global aniline is produced by catalytic hydrogenation of nitrobenzene. The catalytic hydrogenation of nitrobenzene for the production of aniline, can be performed either in vapour phase or in liquid-phase processes. Recently, carbon nanotube supported platinum catalyst has been used for the hydrogenation of nitrobenzene [1]. Platinum nanoparticle core-polyaryl ether trisacetic acid ammonium chloride dendimer shell nanocomposites were also employed for hydrogenation of nitrobenzene to aniline with molecular hydrogen under mild conditions [2]. Active carbons were used as supports for palladium in the liquid phase hydrogenation of nitrobenzene to aniline [3]. Hydrogenation of nitrobenzene was studied over Pt/C catalysts in supercritical carbon dioxide and ethanol [4]. Vapor phase hydrogenation of nitrobenzene is carried out on Pd supported on hydrotalcite catalysts [5]. Liquid phase hydrogenation of nitrobenzene was studied over $Pd\text{-}B/SiO_2$ amorphous catalyst [6].

There is a great interest growing recently on the use of supported metal/metal oxide systems both in fundamental and industrial applications due to its wide spread utility in chemical industry in comparison to the bulk oxides. In these systems support plays a decisive role in dispersing the active component, stabilize the small metallic particles and enhancing the metal support interaction and further the catalytic activity. The influence of supports like TiO_2, Al_2O_3, ZrO_2 and SiO_2 is well established but the development of new supports is of great interest. In recent years the use of SBA-15 mesoporous family offers new perspectives to employ as a catalyst support. SBA-15 is an ordered mesoporous silica with large surface area $>600\ m^2/g$, uniform hexagonal channels ranging from 50 to 300 Å. The main advantage of SBA-15 materials compared to the supports like $Al_2O_3 \cdot SiO_2$ etc. is its thicker walls, larger pore size and remarkable hydrothermal

K. V. R. Chary (✉) · C. S. Srikanth
Catalysis Division, Indian Institute of Chemical Technology, Hyderabad, India
e-mail: kvrchary@iict.res.in

stability [7–9]. These properties exhibited by SBA-15 have attracted considerable attention recently for its potential application in catalysis [9–13] and many catalysts have been prepared by introducing noble metals, and their oxides into the channels of SBA-15. Supported ruthenium catalysts are used in industrial process like F–T synthesis of paraffins [14] methanation of CO [15] or in the selective hydrogenation of benzene to cyclohexane [16]. Recently, ruthenium is found to have very good catalytic activity towards synthesis of ammonia [17]. Ruthenium has its application in the catalytic decomposition of nitrous oxide [18]. Ruthenium is also used in catalytic oxidation of alcohols and amines to corresponding aldehydes and nitriles [19, 20]. Due to versatile applications of Ru in different chemical reactions, in the present investigation we have investigated Ru catalysts supported on SBA-15 with different ruthenium loadings by wet impregnation method. The properties of SBA-15 and Ru/SBA-15 were characterized by BET surface area, pore size distribution, X-ray diffraction (XRD), temperature programmed reduction (TPR), transmission electron microscopy (TEM) and CO-chemisorption measurements. The catalytic properties were explained in terms of the active species measured from CO-chemisorption studies. A comparision is made with Ru supported of Al_2O_3 and SiO_2 for the hydrogenation of nitrobenzene under similar reaction conditions.

2 Experimental

2.1 Preparation of the SBA-15 and Ru/SBA-15

SBA-15 was prepared by the procedure described by Zhao et al. [7, 8]. The SBA-15 silica was prepared using triblock copolymer poly-ethylene glycol–blockpolypropylene glycol–block-poly-ethylene glycol (P123, average molecular mass $\approx$5800 g, Aldrich) as a template. About 2 g of P123 copolymer was dissolved in a mixture of 15 g of water and 45 g of 2 M HCl under stirring followed by the addition of 0.2 g of cetyltrimethyl ammonium bromide (CTMABr) and 5.9 g of tetraethylorthosilicate (TEOS). The final molar ratio was 1 TEOS: 0.02 CTMABr: 3.1 HCl: 115 H_2O: 0.012 polymer. The synthesis mixture was introduced into a plastic bottle, sealed and kept at 373 K for 24 h; then cooled down, filtered and washed with deionised water and ethanol to remove the excess of template prior to calcination. A series of Ru/SBA-15 catalysts with Ru loadings in the range of 0.5–6.0 wt% Ru were prepared by wet impregnation with an aqueous solution containing $RuCl_3 \cdot 3H_2O$ (Aldrich). The samples were subsequently dried at 373 K for 16 h. The samples were reduced in hydrogen (99.9%) flow at 573 K for 3 h and characterized by different characterization techniques.

2.2 X-Ray Diffraction Studies

X-ray diffraction patterns were obtained on Rigaku miniflex diffractometer using graphite filtered Cu Kα ($K = 0.15406$ nm) radiation. Determination of the ruthenium phase was made with the help of JCPDS data files.

2.3 BET Surface Area and Pore Size Distribution

The specific surface area, pore size distribution studies of the prereduced catalysts was estimated using N_2 adsorption isotherms at 77 K by the multipoint BET method taking 0.0162 nm^2 as its cross-sectional area using Autosorb 1 (Quantachrome instruments).

2.4 TEM Analysis

The morphological analysis was carried out using transmission electron microscopy (TEM on a JEOL 100S microscope at high resolution (HR) on a JEOL 2010 microscope). Samples for both TEM analysis were prepared by adding about 1 mg of prereduced sample to 5 mL of methanol followed by sonication for 10 min. A few drops of suspension were placed on a hollow copper grid coated with a carbon film made in the laboratory.

2.5 CO-Chemisorption

CO-chemisorption measurements were carried out on Auto Chem 2910 (Micromeritics, USA) instrument. Prior to adsorption measurements, ca. 100 mg of the sample was reduced in a flow of hydrogen (50 mL/min) at 673 K for 3 h and flushed out subsequently in a pure helium gas flow for an hour at 673 K. The sample was subsequently cooled to ambient temperature in the same He stream. CO uptake was determined by injecting pulses of 9.96% CO balanced helium from a calibrated on-line sampling valve into the helium stream passing over the reduced samples at 673 K. Ruthenium surface area, percentage dispersion and Ru average particle size were calculated assuming the stoichiometric factor (CO/Rus) as 1. Adsorption was deemed to be complete after three successive runs showed similar peak areas.

2.6 Temperature Programmed Reduction (TPR)

Temperature programmed reduction (TPR) experiments were carried out on Auto Chem 2910 (Micromeritics, USA) instrument. In a typical experiment ca. 100 mg of oven dried Ru/SBA-15 sample (dried at 383 K for 12 h) was taken in a U-shaped quartz sample tube. Prior to TPR studies the catalyst sample was pretreated in an inert gas (Argon, 50 mL/min) at 473 K. After pretreatment, the

sample was cooled to ambient temperature and the carrier gas consisting of 5% hydrogen balance argon (50 mL/min) was allowed to pass over the sample raising the temperature from ambient to 673 K heating at the rate of 10 K/min. The HCl produced during the reduction was condensed in a cold trap immersed in liquid nitrogen and isopropanol slurry. The hydrogen concentration in the effluent stream was monitored with the TCD and the areas under the peaks were integrated using GRAMS/32 software.

2.7 X-Ray Photoelectron Spectroscopy

X-ray photoelectron spectroscopy was used to study the chemical composition and oxidation state of catalyst surfaces. The XPS spectra of the catalysts were measured on a XPS spectrometer (Kratos-Axis 165) with Mg Kα radiation (hγ) 1253.6 eV) at 75 W. The Ru 3d and 3p core-level spectra were recorded and the corresponding binding energies were referenced to the C 1s line at 284.6 eV (accuracy within (0.2 eV)). The background pressure during the data acquisition was kept below 10^{-10} bar.

2.8 Catalytic Activity Studies

Hydrogenation of nitrobenzene (≥99.9% Aldrich chemicals) was carried out over the catalysts in a vertical downflow glass reactor at 548 K and operating under atmospheric pressure. About ca. 100 mg of the catalyst, diluted with double the amount of quartz grains was packed between the layers of quartz wool. The upper portion of the reactor was filled with glass beads, which served as pre-heater for the reactants. Prior to the reaction, the catalyst was reduced in a flow of hydrogen (50 mL/min) at 573 K for 3 h. After reduction the reactor was fed with nitrobenzene at 523 K (WHSV = 36.12 h^{-1}; H_2/Nitrobenzene = 4; Residence time : 0.0276 h). The reaction products were analyzed by HP-6890 gas chromatograph equipped with a HP-5 capillary column with a flame-ionization detector (FID). The products were also identified using HP-5973 quadrupole GC-MSD system using HP-1MS capillary column.

3 Results and Discussion

3.1 Characterization Results

The low angle XRD patterns of the synthesized materials are typical for the SBA- 15. Figure 1 illustrates the presence of reflections at 2θ angle of 0.9°, 1.7°, and 1.9°, corresponding to the planes of (100), (110), and (200). Bragg reflections, confirming the hexagonal symmetry (*P6* mm) of the SBA-15 materials prepared [8, 10]. A well-resolved peak at 0.9° and two small peaks at 1.7° and 1.9°

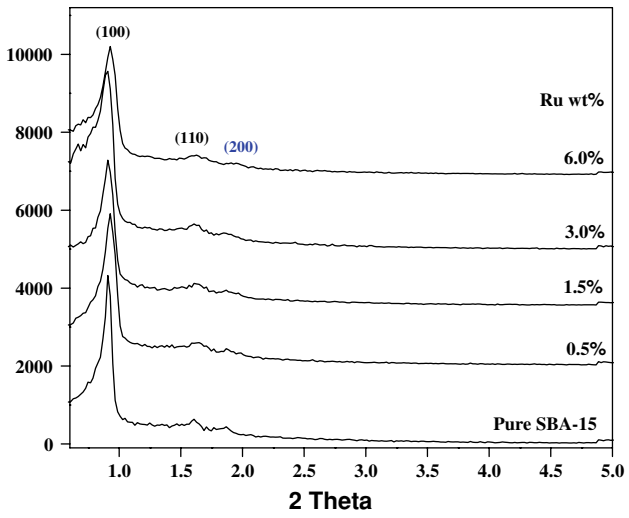

Fig. 1 Low angle XRD patterns of pure SBA-15 and Ru/SBA-15 catalysts

also can be seen for the various Ru/SBA-15 catalysts (Fig. 1). The decrease in the intensity of XRD peaks at 1.7° and 1.9° are due to blocking of the pores of the SBA-15 with the ruthenium. However, it did not significantly change the hexagonal ordering of SBA-15 framework as seen from the BJH isotherms from Fig. 2. Figure 2 shows N2 adsorption–desorption isotherms of pure SBA-15 and Ru/SBA-15 catalysts. All the samples exhibit irreversible type IV adsorption isotherms with an H1 hysteresis loop confirming the presence of mesopore structure [10, 21].

The BET surface areas determined by nitrogen physisorption of all the catalysts are presented in Table 1. The specific surface area of the pure SBA-15 support was found to be 715 m^2/g. The BET surface area decreases as a function of ruthenium loading on SBA-15, and it might be due to surface hydroxyl groups of the support consumed by reaction with the active phase precursor. Such a surface reaction might have caused the decrease of available surface area of the support, probably by closure of the pores as evidenced by PSD. The BJH isotherms of SBA-15 sample before and after impregnation of Ru are shown in Fig. 2a. It demonstrates that the incorporation of ruthenium does not affect the mesoporous structure of SBA-15. Low angle XRD and BJH isotherms suggest that the hexagonal wall structure of SBA-15 was intact even after impregnation with Ru precursor. Total pore volume and total pore area of samples measured by Autosorb-1 (Quantachrome instruments) have also been reported in Table 1, are found to decrease with increase of ruthenium loading in the similar lines of surface area of the catalysts. All samples exhibited uni-model pore size distribution (Fig. 2b).

Powder XRD patterns of SBA-15 and various prereduced Ru/SBA-15 catalysts in the 2θ range of 10°–65° are recorded. All the samples shown (not presented here) a

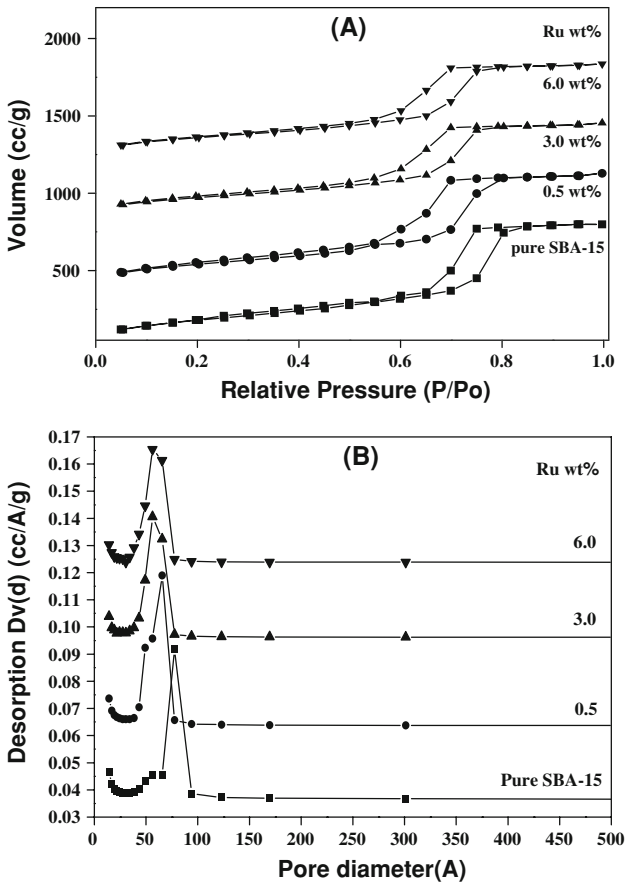

Fig. 2 **a** Nitrogen adsorption–desorption isotherms and pore size distributions; **b** BJH pore size distribution of SBA-15 and Ru/SBA-15 catalysts

Table 1 BET surface are and pore size distribution data of SBA-15 and various Ru/SBA-15 catalysts

Ru wt%	BET surface area (m^2/g)	Pore diameter (nm)	Pore volume (cc/g)
SBA-15	715	7.7	1.24
0.5	702	6.5	1.20
1.5	690	–	–
3.0	679	5.7	1.12
4.5	668	–	–
6.0	648	5.6	1.04

broad reflection ranging from 15°–30° characteristic of amorphous silica [22]. It is also observed that all the samples except pure SBA-15 show a broad reflection at around 44°, which is due to amorphous ruthenium [23]. This peak becomes sharp from 4.5 wt% ruthenium and gave a clear reflection at 6.0 wt% indicating the crystallization of ruthenium beyond 4.5 wt%. This indicates the formation of Ru^0 phase [24]. The XRD result suggests that high dispersion of Ru on SBA-15 was observed below 4.5 wt% Ru in the catalyst. Beyond this loading, the particle size of ruthenium increases due to agglomerization. The physical properties of catalysts such as dispersion, metal surface area and average particle size obtained from CO-chemisorption are given in Table 2. The dispersion of Ru was calculated from CO-chemisorption using the following equation assuming the cubic particle with five sides exposed to the gas plane,

$$\%\ \text{Dispersion} = \big(\text{Number of surface ruthenium atoms} \times 100\big)\big/ \text{Total number of ruthenium atoms.}$$

$$\text{Average particle size}\big(\text{nm}\big) = 6000\big/\big(\text{Ru metalarea per gram of Ru} \times \text{Ru density}\big).$$

The ruthenium metal areas were determined using the equation $S_{CO} = nm^S\ X_m\ ns^{-1}$, where S_{CO} is the total metallic surface area, nm^S is the CO consumption and X_m is chemisorption stoichiometry at monolayer coverage, and ns-1 is the number of ruthenium atoms per unit surface area. The results shown in Table 2 clearly suggest that ruthenium dispersion and metal surface area decrease with increase of Ru loading. The crystallite size of ruthenium increases with ruthenium loading due to the agglomerization of ruthenium particle, which is in good agreement with TEM and XRD. From the CO uptake values it is clear that the number of active sites of ruthenium available on SBA-15 increases up to 4.5 wt % and decreases beyond due to the formation of larger particles of ruthenium as evidenced from TEM and XRD.

TEM is a powerful technique to investigate the particle size and distribution. The impregnation of ruthenium particles on to SBA-15 support can lead to deposition on the external surface or confined to channels. The particle sizes of the prereduced Ru/SBA-15 catalysts are estimated from TEM and CO-chemisorption. The TEM images are presented in Fig. 4 and corresponding particle sizes are given in Table 2. As shown in Fig. 3, the TEM images of Ru/SBA-15 samples reveal the highly dispersed Ru particles confined to channels of SBA-15. The average particle size of ruthenium particles estimated from CO-chemisorption is in good agreement with that estimated from TEM results.

The H_2-TPR technique is used to study the reduction behavior of $RuCl_3$, as well as to obtain the information regarding the interaction between the metal and support. The H_2-TPR profiles of different ruthenium loadings supported on SBA-15 are presented in Fig. 4 and the results are presented in Table 3. All the samples have shown a main reduction peak at T_{max} around 360–390 K due to the reduction of Ru^{3+}/Ru^0. These peaks are broad possibly due to location of ruthenium ions in different environments. But at low ruthenium loading (0.5 wt %) the signal was

Table 2 Results of CO-chemisorption and TEM of various Ru/SBA-15 catalysts

Ru wt%	CO uptake (μmol/g)	(%) Dispersion	Metal surface area $(m^2/g)_{Ru}$	Particle size[a] (nm)	Particle size[b] (nm)
0.5	49.43	99.94	486.5	0.99	0.8
1.5	73.12	49.27	239.9	2.01	1.8
3.0	108.99	36.72	178.7	2.70	–
4.5	113.55	25.50	124.1	3.89	4.0
6.0	93.89	15.81	77.0	6.24	6.8

[a] Determined from CO uptake values

[b] Determined from TEM analysis

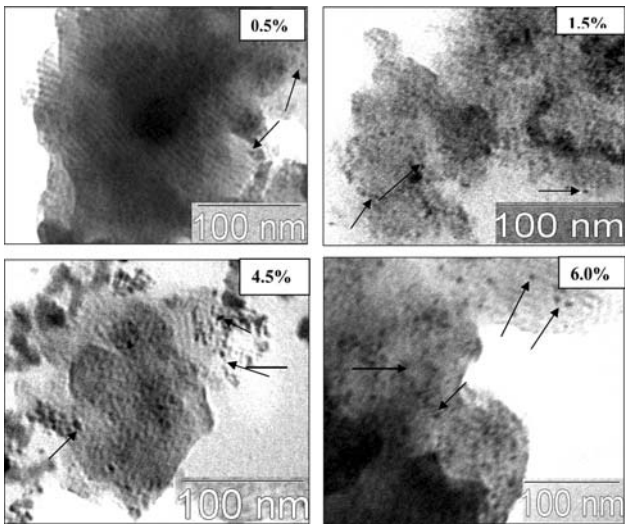

Fig. 3 TEM images of various Ru/SBA-15 catalysts

split in two (α,β) and these peaks are with in the range of first T_{max} of the other samples. The first peak in TPR of these low loading samples (0.5 wt% Ru) is due to stepwise reduction of supported ruthenium chloride [16, 27] All the samples show a second reduction peak at T_{max} around 473 K due to reduction of oxychlorides of ruthenium formed due to air exposition during the preparation of the catalysts [25, 26]. The high temperature peak around 550 K is attributed to the reduction of Ru^{3+} strongly interacting with the support and possibly located in the narrow pores [27].

The catalyst surface composition and the oxidation state of prereduced Ru/SBA-15 catalysts were investigated by using XPS. In XPS analysis, Ru 3p signals were considered instead of 3d signals to find the exact oxidation state of ruthenium, as the Ru 3d signal overlap with C 1s signal. The 3p signal shows a doublet at B.E. 462.0 and 484.3 (eV), which are characteristic of Ru^0 [27]. The B.E. of $3p_{3/2}$ at 462.5 (eV) for 0.5 wt% shifts to 462.0 (eV) for 6.0 wt%. This suggests that the decrease in metal support interaction between ruthenium and SBA-15 with increasing metal loading. The XPS further confirms the absence of

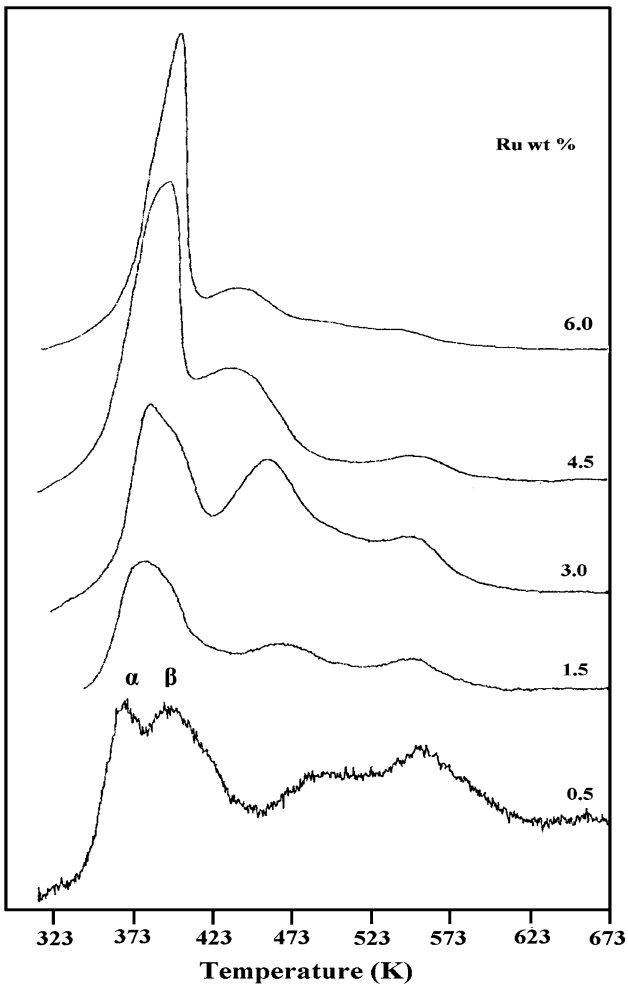

Fig. 4 H2 TPR profiles of various Ru/SBA-15 catalysts

any surface Cl species. TPR results also show that the reduction of the samples complete before 573 K due to complete reduction to metallic state of ruthenium.

3.2 Activity Results

The catalytic properties of Ru/SBA-15 catalysts were evaluated during the vapor phase hydrogenation of

Table 3 TPR data of various Ru/SBA-15 catalysts

Ru wt%	Tmax[1]	H_2 uptake μmol	Tmax[2]	H_2 uptake μmol	Tmax[3]	H_2 uptake μmol	Tmax[4]	H_2 uptake μmol	Total H_2 uptake μmol
0.5	363	31.0	383	43.6	498	62.4	554	176	313
1.5	378	177	–	–	473	114	550	100	391
3.0	381	229	–	–	452	229	547	105	563
4.5	388	431	–	–	438	252	544	107	790
6.0	393	683	–	–	442	274	532	104	1061

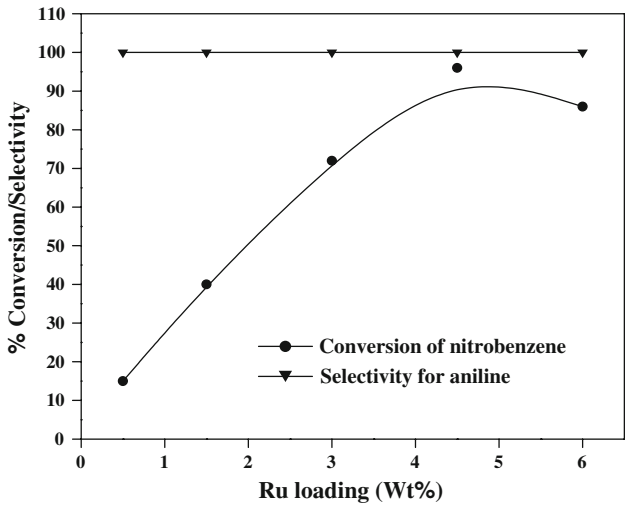

Fig. 5 Hydrogenation of nitrobenzene to aniline over Ru/SBA-15 catalysts reaction conditions: weight of the catalyst = 100 mg; reaction temperature = 548 K; WHSV = 36.12 h^{-1}; H_2/Nitrobenzene = 4; residence time: 0.0276 h

nitrobenzene to aniline at 548 K. The main reaction product obtained was aniline with trace amounts of benzene. The effect of ruthenium loading on SBA-15 for the hydrogenation activity is shown in Fig. 5. the conversion values reach a maximum between 4.0 and 6.0% Ru loading. This is in good agreement with the CO uptake value wherein the uptakes increase up to 4.5 wt% and decrease for 6 wt% of ruthenium. All the catalysts show >99% selectivity towards the formation of aniline. The conversion during hydrogenation of nitrobenzene was found to increase with increasing ruthenium loading up to 4.5 wt% and decreased at 6 wt%. The activity of the catalysts at lower loadings (0.5 and 1.5 wt%) is rather low due to their strong interaction with SBA-15 as seen form the TPR patterns showing multiple and broad peaks indicating the presence of ruthenium in different environments. The possibility is that the ruthenium particles can be confined deep in the channels of SBA-15 and cannot participate in the reaction, while those Ru particles positioned at or near the pore opening act as a reaction site.

A comparison is made for the results of dispersion, metal area specific surface area and the hydrogenation activity of the present study with 4.5 wt% Ru on Al_2O_3 and SiO2 (Table 4). The characterization and the catalytic experiments are conducted under similar experimental conditions as employed for Ru/SBA-15 catalysts. The results suggest that Ru/SBA-15 has shown high dispersion, metal area and superior activity than the other catalysts. The high metal area of Ru/SBA-15 catalysts makes the metal surface more accessible to the CO-chemisorption and the hydrogenation activity. The high surface area and intact pore structure of SBA-15 favors high dispersion and metal area of the active component, which further enhances the catalytic activity. However, the selectivity for the formation of aniline is similar for Ru/SiO_2 and Ru/SBA-15.

The high catalytic activity exhibited by Ru/Al_2O_3 compared to Ru/SiO_2, despite of having low surface area and dispersion can be probably explained as follows. The catalytic activity during hydrogenation is not influenced by dispersion. Al_2O_3 adsorbs more chlorine than SiO_2 from the ruthenium precursor, due to which electron deficient ruthenium is present in Ru/Al_2O_3 catalysts than on Ru/SiO_2. The electron deficient Ru on Al_2O_3 desorbs the aniline easily than SiO_2 and thus allows more nitrobenzene molecules to convert. An explanation similar to the above is given by Mazzieri et al. [28] in his recent work on selective hydrogenation of benzene to cyclohexene over Ru supported silica and alumina catalysts.

Table 4 Comparison table for BET surface area and activity of ruthenium catalysts

Catalyst (4.5 wt%)	BET surface area (m^2/g)	% Dispersion	Metal area $(m^2/g)_{Ru}$	% Conversion	% Selectivity
Ru/SBA-15	668	25.5	124.1	96.5	99.9
Ru/SiO_2	304	20.8	101.3	60.2	98
Ru/Al_2O_3	160	10.3	50.3	85.0	92

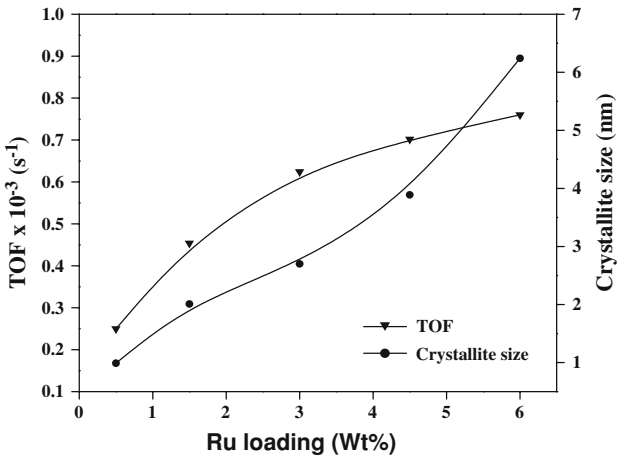

Fig. 6 Relationship between Ru loading, TOF and particle size for hydrogenation of nitrobenzene

Figure 6 shows the relation between TOF (number of molecules of nitrobenzene converted per second per site), particle size and ruthenium loading. The TOF values increase up to 3.0 wt% of ruthenium and levels off at higher loadings. The particle size of ruthenium also increases smoothly up to 4.5 wt% and tend to increase exponentially at 6 wt%. This clearly shows that the conversion of nitrobenzene is directly related to the number of active sites available determined from CO-chemisorption. The increase in the crystallite size beyond 4.5 wt% indicate that the overloading of the metal lead to the increase in the crystallite size due agglomerization of ruthenium particles but will not increase the number of active sites. The catalytic samples between 4.0 and 6.0 wt% Ru exhibited the higher activity than other Ru/SBA-15 catalysts. The leveling off of the TOF at higher Ru loadings is attributed to the decrease in the number of active sites of ruthenium on SBA-15 due to agglomerization as evidenced from the results of XRD, TEM and CO-chemisorption measurements.

4 Conclusions

Highly dispersed ruthenium catalysts can be prepared confined to channels of SBA-15 support by the impregnation method. Ruthenium supported SBA-15 catalysts exhibit high catalytic activity for the hydrogenation of nitrobenzene. Moreover, high selectivity towards the formation of aniline makes Ru more promising for hydrogenation of nitrobenzene reaction. Low angle XRD and pore size distribution confirms that the pore structure of SBA-15 remains intact even after the introduction of ruthenium. XRD results also show the presence of Ru0 from 4.5 wt%, which is further supported by the TEM and CO-chemisorption measurements. XPS reveals the formation of Ru^0 after reduction at 573 K and in good agreement with TPR results. The catalyst with 4.5 wt% Ru is found to be optimum loading for the conversion of nitrobenzene beyond which the particle size of ruthenium increases leading to decrease in the number of active sites and decrease of catalytic activity. Ru supported on SBA-15 exhibits higher activity during nitrobenzene hydrogenation than Ru supported on alumina or silica. The catalytic activity is directly related to the CO-chemisorption sites.

Acknowledgements The authors thank Director, IICT, Hyderabad for his encouragement. Ch. S. S thanks CSIR, New Delhi for the award of Senior Research Fellowship.

References

1. Li CH, Yu ZX, Yao KF, Ji SF, Liang J (2005) J Mol Catal A: Chem 226:101
2. Yang P, Zhang W, Du Y, Wang X (2006) J Mol Catal A: Chem 260:4
3. Bouchenafa-Saib N, Grange P, Verhasselt P, Addoun F, Dubois V (2005) Appl Catal A: Gen 286:167
4. Zhao F, Ikushima Y, Arai M (2004) J Catal 224:479
5. Sangeetha P, Seetharamulu P, Shanthi K, Narayanan S, Rao KSR Jr (2007) Mol Catal A: Chem 273:244
6. Yu X, Wang M, Li H (2000) Appl Catal A: Gen 202:17
7. Zhao DY, Feng J, Huo Q, Melosh N, Fredrickson GH, Chmelka BF, Stucky GD (1998) Science 279:548
8. Zhao DY, Huo Q, Feng J, Chmelka BF, Stucky GD (1998) J Am Chem Soc 120:6024
9. Du G, Lim S, Pinault M, Wang C, Fang F, Pfefferle L, Haller GL (2008) J Catal 253:74
10. Lihui Z, Jun H, Songhai X, Honglai Chin L (2007) Chem Eng J 15(4):507
11. Liu Yong-Mei, Cao Y, Yi N, Feng Wei-Liang, Dai Wei-Lin, Yan Shi-Run, He He-Yong, Fan Kang-Nian (2004) J Catal 224:417
12. Rioux RM, Song H, Hoefelmeyer JD, Yang P, Somorjai GA (2005) J Phys Chem B 109:2192
13. Tu Cai-Hua, Wang Ai-Qin, Zheng Ming-Yuan, Wang Xiao-Dong, Zhang T (2006) Appl Catal A: Gen 297:40
14. Iglesia E, Soled SL, Fiato RA, Via GH (1993) J Catal 143:345
15. Vander Wiel DP, Pruski M, King TS (1999) J Catal 188:186
16. Mazzieri V, Coloma-Pascual F, Arcoya A, Argentiere PCL, Figoli NS (2003) Appl Surf Sci 210:222
17. Zhang J, Xu H, Ge Q, Li W (2006) Catal Comm 7:148
18. Kawi S, Liu SY, Shen SC (2001) Catal Today 68:237
19. Yamaguchi K, Mizuno N (2002) Angew Chem 41:4538
20. Yamaguchi K, Mizuno N (2003) Angew Chem 42:1480
21. Sing KSW, Everett DG, Haul WAW, Moscow L, Pierotti RA, Rouquerol J, Siemieniewska T (1985) Pure Appl Chem 57:603
22. Cho YS, Park JC, Lee B, Kim Y, Yi J (2002) Catal Lett 81:89
23. Lee Der-Shing, Liu Tsung-Kwei (2002) J Non-Cryst Solids 311:323
24. Barbier J Jr, Delanoe F, Jabouille F, Duprez D, Blanchard G, Isnard P (1998) J Catal 177:378
25. Betancourt P, Rives A, Hubaut R, Scott CE, Goldwasser J (1998) Appl Catal A: Gen 170:307
26. Koopman PGJ, Kieboom APG, van Bekkum H (1981) J Catal 69:172
27. Quesada DE, Ortiz MIM, Jimenez JJ, Castellon ER, Lopez AJ (2006) J Mol Catal A: Chem 255:41
28. Mazzieri V, Figoli N, Pascual Fernando-Coloma, L'Argentiere P (2005) Catal Lett 102:79